PASJ: Publ. Astron. Soc. Japan **44**, 353–365 (1992)

High-Resolution CO Observations of the Radio-Lobe Edge-on Galaxy NGC 3079

Yoshiaki SOFUE
Institute of Astronomy, The University of Tokyo, Mitaka, Tokyo 181
and
Judith A. IRWIN
Herzberg Institute of Astrophysics, National Research Council of Canada, 100 Sussex Drive, Ottawa, Ontario, K1A 0R6, Canada

(Received 1991 October 2; accepted 1992 March 12)

Abstract

We have performed high-resolution ^{12}CO ($J = 1-0$) observations of the radio lobe spiral galaxy, NGC 3079. The molecular gas is distributed in a disk comprising (a) an unresolved nuclear core showing high-velocity dispersion, (b) a rigidly rotating broad nuclear ring of radius $\sim$ 190 pc, which extends to about 750 pc radius, and (c) an outer disk showing spiral arm structures. The inner part of the nuclear ring is significantly warped about 40° from the major axis, and is associated with two vertical spurs which extend toward the radio continuum lobes. The kinematics and morphology of the molecular nuclear disk are discussed in relation to the radio lobe activity.

Key words: CO emission — Galaxies: individual (NGC 3079) — Jets — Nuclear activity

1. Introduction

NGC 3079 is the prototype of a loosely defined "class" of spiral galaxies which exhibit radio lobes emerging from their nuclei (Hummel et al. 1983). The evidence, to date, suggests that nuclear outflow originates with accretion onto a compact core (Irwin and Seaquist 1988), similar to such Seyfert galaxies as NGC 1068, rather than with star formation, as observed in M82 (e.g., Nakai et al. 1987). However, only a few such galaxies are currently known (e.g., NGC 1808: Véron-Cetty and Véron 1985); details concerning the ejection mechanism, as well as the complex interplay between the ISM, central engine, and outflow, itself, are far from clear.

NGC 3079 has been studied in some detail at a number of wavebands (Duric et al. 1983; Ford et al. 1985; Irwin et al. 1987; Duric and Seaquist 1988; Irwin 1988; Irwin and Seaquist 1988; Young et al. 1988). The line widths of CO (Young et al. 1988), OH (Haschick and Baan 1985), and H I (Irwin 1988; Irwin and Seaquist 1991), obtained at different spatial resolutions are far in excess of the normal galactic rotational velocities, and are undoubtedly associated with the nuclear gas. Relatively high-resolution observations from the Owens Valley mm-wave array infer the existence of a dense nuclear molecular disk within the central 14″ (Young et al. 1988).

NGC 3079 is a galaxy whose unusual nuclear activity can be probed by observing the affected interstellar medium. In particular, high-resolution CO observations are required to determine how the morphology and kinematics of the nuclear molecular disk are related to the nuclear activity. The distribution of molecular gas is also of interest, since the nuclear outflow appears to dramatically change direction within about 4″ of the nucleus (Irwin and Seaquist 1988). In this paper we report on the results of high-resolution CO observations of NGC 3079 using the NRO mm-wave interferometer.

2. Observations and Data Reduction

The ^{12}CO (1–0) observations of NGC 3079 were made using the NMA (Nobeyama 5-element mm-wave array) in the C and D (compact) configurations. C-array observations were made on 1991 January 28–29 and 1991 February 4–5 1991, and D-array observations on 1991 January 4–5 and 13–14. The UV coverage of the observations was almost ideal for a 5-element interferometer. The synthesized main beam had a HPBW of $4''.07 \times 3''.55$ at a position angle of 85°. At a distance of 15.6 Mpc (for the galacto-centric H I systemic velocity as below with $H_0 = 75$ km s^{-1} Mpc^{-1}) this resolution corresponds to 305 pc × 266 pc ($1'' = 75$ pc)

The center position of the galaxy was taken to be at RA = $09^h58^m35^s.02$ and Dec = $55°55'15''.4$ (epoch 1950). The phase and band-pass calibrations were made while observing radio sources 1012+232 and 3C 84, respectively. The flux calibration was made by observing 0923+392, which had a flux density of 4.6 Jy at

109.8 GHz on January 10, compared to radio source 3C 273=30.0 Jy, and 4.6 Jy at 114.3 GHz on February 1 when 3C 273=31.0 Jy. The intensity was calibrated by observing the planet Uranus whose brightness temperature was assumed to be 130 K.

The center frequency was 114.843360 GHz, corresponding to the LSR recession velocity of the galaxy, $V_{\rm LSR}$ = 1113 km s^{-1} (LSR) according to the radio definition. This is approximately the same as the H I systemic LSR velocity, 1116 km s^{-1} (galacto-centric velocity 1168 km s^{-1}), as derived by Irwin and Seaquist (1991). The data acquisition was made with SIS receivers equipped on each antenna. A 1024-channel FX system (a fast-Fourier-transform spectro-correlator: Chikada et al. 1987) was used for the spectroscopic data acquisition with a total bandwidth of 320 MHz (831 km s^{-1}). The data were averaged in 16 bins of original frequency channels to achieve a velocity resolution of 13 km s^{-1}; they were then converted to visibility and UV data on a FACOM VP200 vector processor. The data subsequently comprised 64-channels covering 320 MHz with a frequency (velocity) resolution of 5 MHz (13 km s^{-1}). These data were Frourier transformed to the image plane, and then CLEANed using the AIPS reduction system.

3. Results

3.1. CO Spectra

Figure 1a shows the obtained spectra for the central area of NGC 3079. Here, the galactic center is at the center of the diagram, and the major axis of the galaxy (position angle of $-15°$) is parallel to the ordinate direction; the minor axis is in the abscissa direction. Brightness temperatures as high as 5–9 K were observed near the nucleus. The highest temperature of 9.3 K was recorded toward a point $\sim 3''$ to the north of the nucleus at $V_{\rm LSR}$ =1154 km s^{-1}. The velocity width is very large toward the nucleus, where a maximum width of about 750 km s^{-1} is observed. The mean velocity varies along the major axis, which indicates galactic rotation. We can recognize various kinematical components in the profiles; these are discussed separately in the following subsections using more convenient data displays.

We mention an absorption feature at $V_{\rm LSR}$ =1150 km s^{-1}, which can be clearly recognized only on the spectrum toward the nucleus. The depth is about 2.5 K in $T_{\rm B}$, about ten sigma of rms noise. Since we used an FX system for the spectral data acquisition, not a filter bank, the feature is real. The line width of this absorption feature is less than 13 km s^{-1}, and its mean velocity coincides with the CO systemic velocity, as discussed later. Moreover, the feature appears to be very local, associated only with the strong emission from the nucleus. From these facts it may be argued that the feature is most likely to be due to absorption by a foreground molecular cloud in the disk, which is either circularly rotating around the nucleus or moving perpendicularly to the line of sight. Judging from the small velocity width ($<$ 13 km s^{-1}) and from the proximity to the systemic velocity, it is not likely that the cloud is closely associated with the nucleus: gas clouds near the galactic center usually have a large velocity dispersion. From these arguments, the cloud may most probably lie in the outer disk, perhaps in a spiral arm. We note that such absorption features caused by foreground molecular clouds in the outer disk and spiral arms are usually observed toward our Galactic Center. We also mention that similar narrow absorption features in CO have been detected toward the starburst galaxy M82 (Nakai et al. 1986) and the radio galaxy NGC 5128 (Cen A) (Eckart et al. 1990; Israel et al. 1990).

3.2. Total Intensity Map

Figure 2 shows the integrated intensity map of NGC 3079 in the CO line, as obtained by integrating the channel maps in figure 3. The nuclear molecular disk is clearly elongated at a position angle of $-15°$, which is the direction of the major axis of the optical and radio continuum disk. The disk comprises three major components:

(a) An innermost compact component having a sharp peak with an extent of $5''$ (375 pc), slightly elongated in the direction of the major axis (not fully resolved yet).

(b) A nuclear disk of radius about $10''$ (750 pc), elongated in the direction of the optical major axis. The central part appears to be associated with spur features extending perpendicular to the disk.

(c) An outer disk extending for more than $X = \pm 30''$ ($\pm$2.2 kpc) along the major axis, where X is the distance from the nucleus along the major axis; it is positive toward the south-east ($PA = 165°$). This component is better seen in the channel maps shown below (figure 3).

3.3. Channel Maps

Figure 3 shows channel maps at velocities of $V_{\rm LSR}$ =748, 852, ..., 1164, ..., and 1478 km s^{-1} integrated every 104 km s^{-1}. All of the components noticed in the total intensity map (figure 2) are also visible in these maps in greater or lesser proportion from the north to south as the velocity increases. This indicates galactic rotation, with the southern disk recessing and the northern disk approaching. In particular, the main disk component, extending up tp $X = -30''$, is clearly seen at $V_{\rm LSR}$ = 1060 km s^{-1} and $+30''$ at 1268 km s^{-1}. This main disk feature is in good positional agreement with the 1.4 GHz radio continuum disk feature (Duric et al. 1983).

Most conspicuous in this figure is the warping nuclear disk appearing in the map at $V_{\rm LSR}$ =1164 km s^{-1}: the

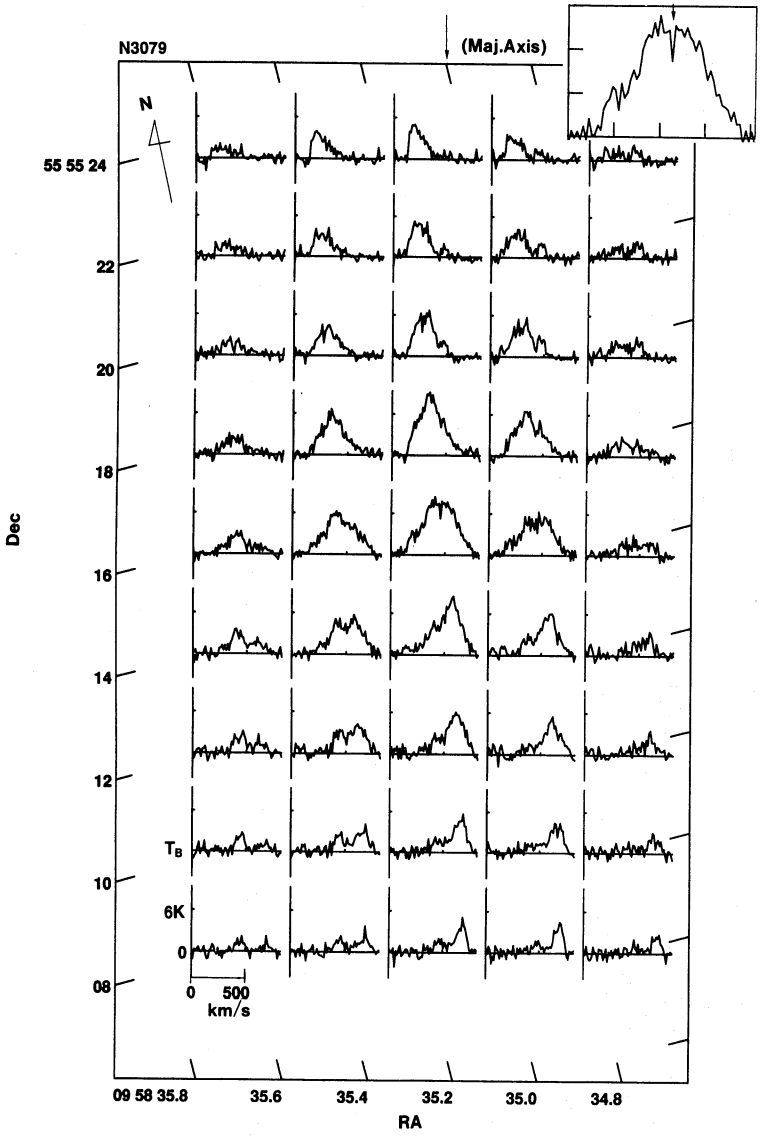

Fig. 1. CO spectra for the central region of NGC 3079. The spectrum toward the nucleus is enlarged in the top-right corner. Note the large velocity width and the sharp absorption feature at $V_{\rm LSR}$ =1150 km s^{-1} (arrowed) toward the nucleus.

disk is significantly inclined from the major axis by about 40°; namely, the disk is elongated in the direction of $PA = -55°$. Also, spur-like features are visible extending perpendicular to this warped disk. In order to isolate these peculiar features, we show channel maps at a higher velocity resolution (every 13 km s^{-1}) in figure 4. The features are most clearly visible on the map at 1158 km s^{-1}, where the warped nuclear disk and the vertical spurs form an inclined "cross." Note that the systemic velocity, as determined from the present CO data for the central region of NGC 3079, is about 1150 km s^{-1}, as is discussed in the next subsection: the "cross" appears most clearly at the CO systemic velocity. The warped disk can be traced from 1067 to 1210 km s^{-1} with its clearest appearence at 1158 km s^{-1}. The vertical spurs are visible on maps from 1080 km s^{-1} to 1158 km s^{-1}, though not so clearly as the warped disk.

We stress that the spurs are extending in the directions of the major radio ridges, which connect the nucleus with the eastern and western radio continuum lobes (Duric et al. 1983); the radio ridges are perpendicular to the warped nuclear disk. It should also be noticed that the warped disk is almost parallel to the north-western extension of the VLBI jet (Irwin and Seaquist 1988). A detailed discussion of this cross feature in relation to the radio continuum ejection features is given in a separate

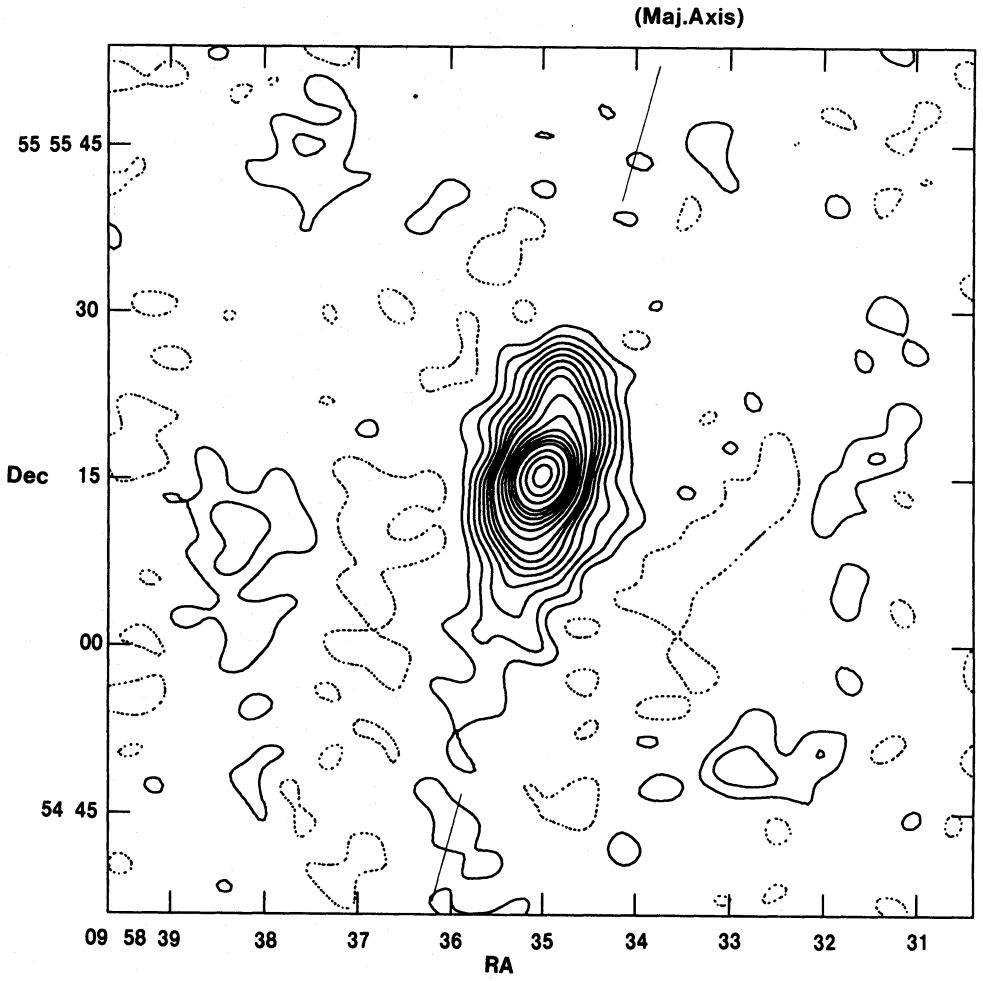

Fig. 2. Total intensity map of the ^{12}CO(J = 1–0) line of NGC 3079, where the intensity scale is the velocity-averaged brightness temperature over 700 km s^{-1} around the center frequency. The peak brightness temperature toward the nucleus is 5.13 K$T_{\rm B}$, which corresponds to $I_{\rm CO}$ = 5.13 × 700 K km s^{-1}. The contour unit is 0.3 K$T_{\rm B}$, and contours are drawn at −0.5, 0.5, 1, 1.5, ..., 3.5, 4, 5, ..., 9, 10, 12, ..., 18, and 20 units. The rms noise level is about 0.05 K.

paper (Irwin and Sofue 1992).

3.4. *Position-Velocity Diagrams*

In order to investigate the kinematical characteristics of the CO gas we make position-velocity (PV) diagrams. Figures 5a to c show PV diagrams parallel to the major axis (galactic plane) [(X, V) diagrams] taken at Z = +4, 0″ and −4″ (+300, 0 and −300 pc), respectively, with Z being the distance perpendicular to the galactic plane and positive toward the north-east (i.e., PA = 75°). Figure 5d is a PV map averaged from $Z = -4''$ to $+4''$ in a gray scale presentation.

(a) *Systemic velocity*: It is readily seen that the PV diagram along the major axis is asymmetric about the adopted center velocity, $V_{\rm LSR}$ =1114 km s^{-1}. The (X, V) diagram approximately becomes symmetric if we adopt a CO systemic velocity of $V_{\rm sys,CO}$ = 1150 km s^{-1} (LSR). Hereafter, we use this new CO systemic velocity. Note that the systemic velocity in CO corresponds to the velocity of the "cross" feature comprising the warped disk and vertical spurs, as described in subsection 3.2. We also mention that the CO systemic velocity is slightly different from that of H I [1125 km s^{-1} (LSR): Irwin and Seaquist 1991], which represents the systemic velocity of the entire galaxy including an outermost H I envelope.

(b) *Nuclear "ring" in rigid rotation*: The main part of the nuclear disk shows an inclined ridge in the (X, V) diagrams, representing rigid rotation with dV/dX = 61.5 km s^{-1} arcsec^{-1} = 820 km s^{-1} kpc^{-1}. The disk has two maxima at around $V_{\rm LSR}$ =1280 and 1050 km s^{-1}, respectively, with a broad depression around the systemic velocity, in addition to the sharp absorption feature, as

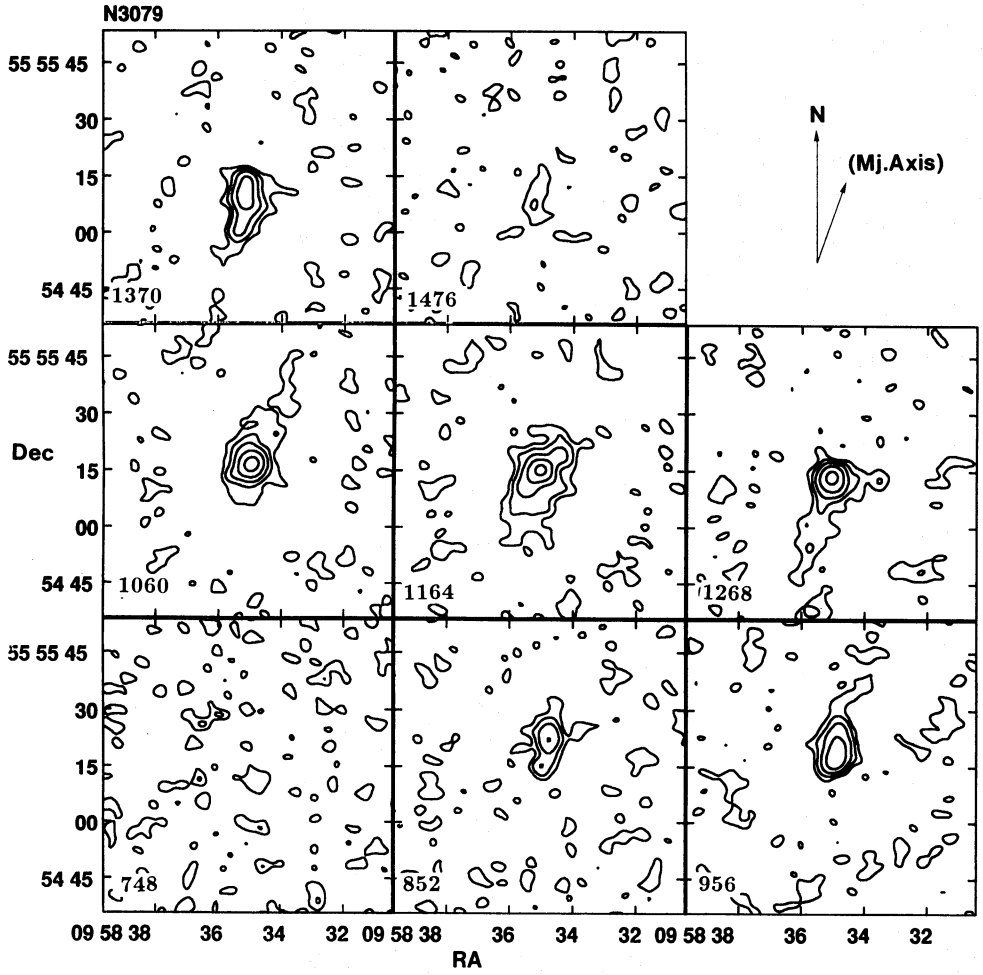

Fig. 3. Channel maps integrated over each 104 km s^{-1} velocity range shown at $V_{\rm LSR}$ = 748, 852, 956, 1060, 1164, 1268, 1372, and 1476 km s^{-1} from bottom-left to right. Contours are drawn at 1, 2.5, 5, 10, and 20 in unit of 0.3 K$T_{\rm B}$. The rms noise is about 0.1 K.

mentioned in subsection 3.1. (figure 1). The spatial separation of the two intensity maxima is approximately 5″ (375 pc). This fact indicates that the feature is not a filled disk, but is a rigidly rotating broad ring with a radius of about 190 pc for the adopted distance of 15.6 Mpc. The nuclear ring on the (X, V) diagram extends up to 1470 and 820 km s^{-1} (+320 and −330 km s^{-1}), so that the disk (ring) is rotating at a maximum velocity of 330 km s^{-1} at $r \sim 400$ pc. After attaining this maximum velocity, the rotation velocity gradually decreases. The entire extent of this disk (ring) component on the (X, V) diagram is about ±20″, or the total radius is about ±750 pc.

(c) *Central compact core*: The main ridge of the nuclear disk on the (X, V) diagram appears to be associated with high-velocity "shoulders" at $V_{\rm LSR} = 850$ km s^{-1} and 1450 km s^{-1} at Dec = 55°55′15″, although the feature is not well resolved (figure 5b). These shoulders may correspond to a compact central core, as desribed in subsection 3.2. (a). Evidence for other non-circular motions near the nucleus are also present: for example, the redshifted H I absorption component ($V_{\rm LSR} \sim 1250$ km s^{-1}), or the lack of symmetry in the OH profiles (Irwin et al. 1991).

(d) *Outer disk (±15″ feature) and spiral arms*: The (X, V) diagrams (figure 5a–d, in particular figure 5d) show two fainter ridges with smaller relative velocities, bifurcating from the main ridge of the nuclear disk; these are significant at more than five rms noise. One ridge runs toward the south at positive velocities (toward top-left in figure 5d) and the other toward the north at negative velocities (toward bottom-right). These bifurcated ridges show a roughly rigid rotation, but at slower velocities. By analogy to the longitude-velocity diagrams of

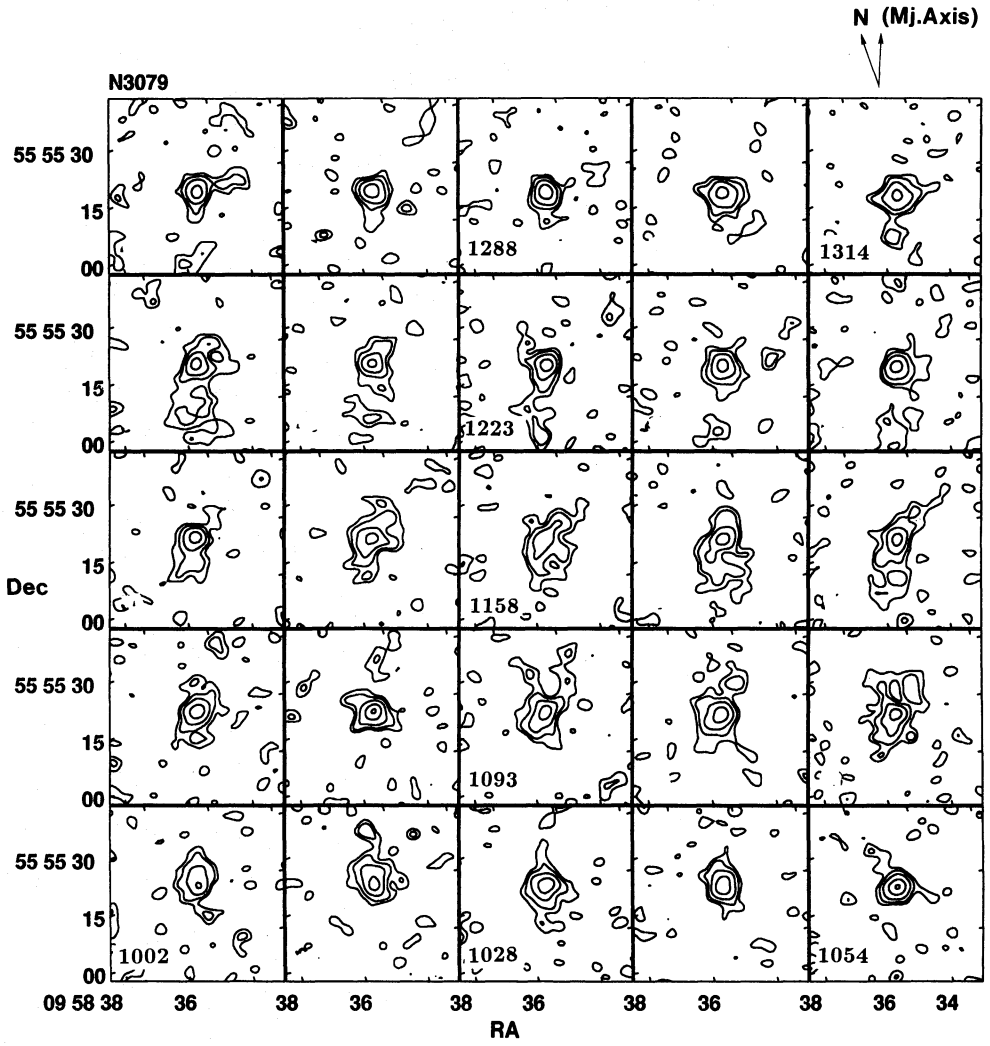

Fig. 4. Channel maps at velocity interval of 13 km s^{-1} from $V_{\rm LSR}$ =1002 km s^{-1} at the bottom-left to 1314 km s^{-1} (top-right). Contours are drawn at 2.5, 5, 10, 20, and 30 in unit of 0.3 K$T_{\rm B}$. The rms noise level is about 0.2 K. Note that the maps have been rotated by 15° so that the major axis of the galaxy is vertical in each map, in order to demonstrate the warped features in the nuclear disk.

our Galaxy, these features may be interpreted as representing spiral arms (or rings). We further notice that the systemic velocity of the southern (left) outer arm is blue-shifted by about 30 km s^{-1} with respect to the CO systemic velocity, and approximately coincides with the H I systemic velocity of 1124 km s^{-1} (Irwin and Seaquist 1991). On the other hand, the northern (right) outer arm is red-shifted by about the same amount. This situation is clearly seen in the gray-scale plot of figure 5d. Such a symmetric velocity displacement between two arm-like features from the nuclear (CO) systemic velocity may represent an expanding or contracting motion of the arms (ring) in the outer disk.

(e) *Rotation curve*: A rotation curve for the inner few kpc of NGC 3079 can be derived from the position-velocity diagrams, as is shown in figure 6. The rotation is almost rigid within r = 400(5″) pc, at which V = 330 km s^{-1}. After attaining the maximum, it gradually decreases and reaches a flat rotation of $V \sim$ 240 km s^{-1} at r = 30–40″ (=2–3 kpc). For a discussion of the larger-scale H I rotation curve, see Irwin and Seaquist (1991).

The CO rotation curve is smoothly continued to an H I rotation curve in the outermost region [$r < 300''$(22 kpc)]; the detailed rotation characteristics of the entire galaxy will be discussed in a separate paper.

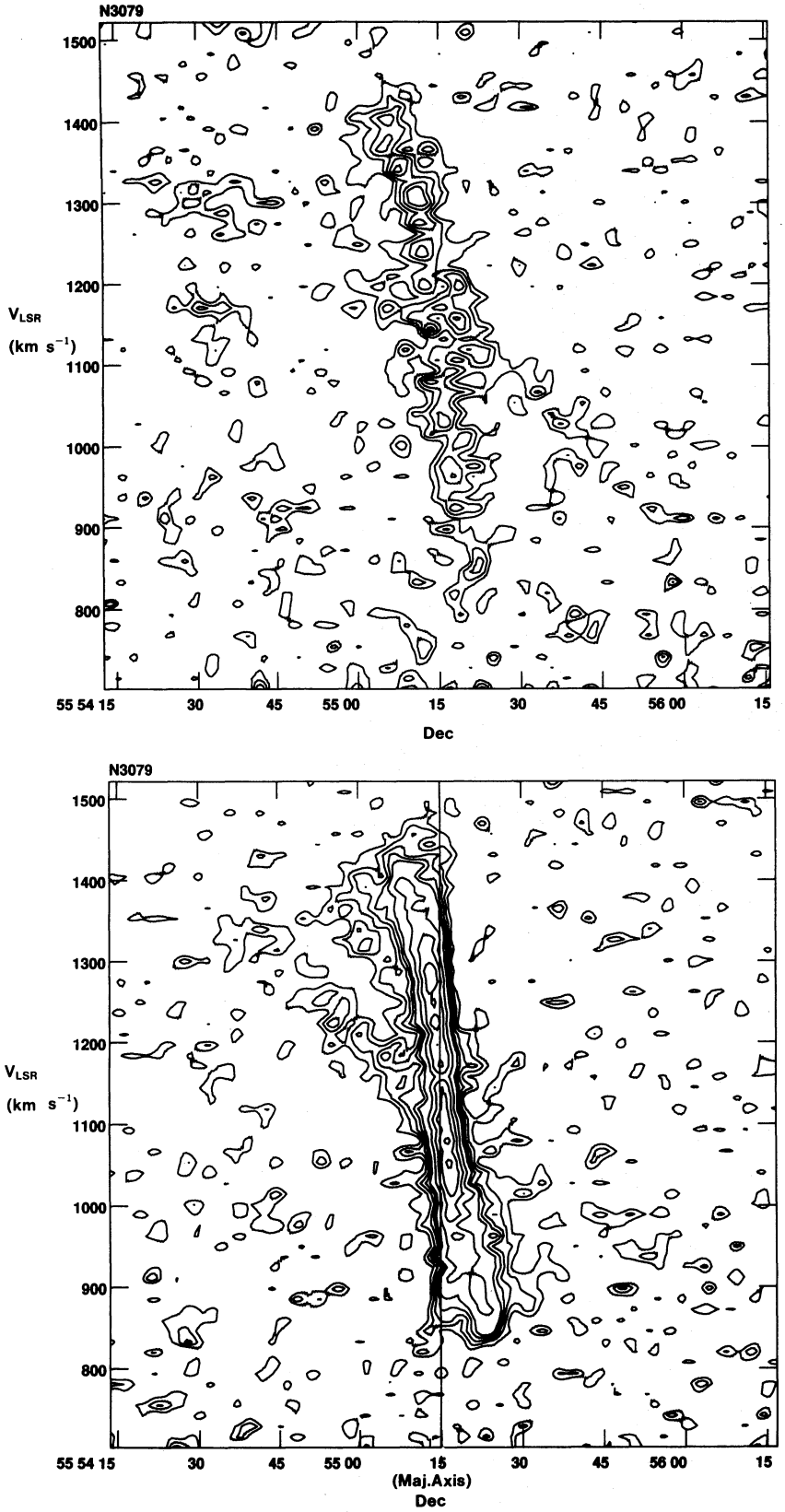

Fig. 5. Position-velocity (X, V) diagrams obtained parallel to the major axis at (a) $Z = +4''(+300)$ pc, (b) $0''$, and (c) $Z = -4''(-300)$ pc (contour levels are the same as in figure 3, and (d) an averaged PV map between $Z = \pm 4''$ in a gray-scale representation.

(c)

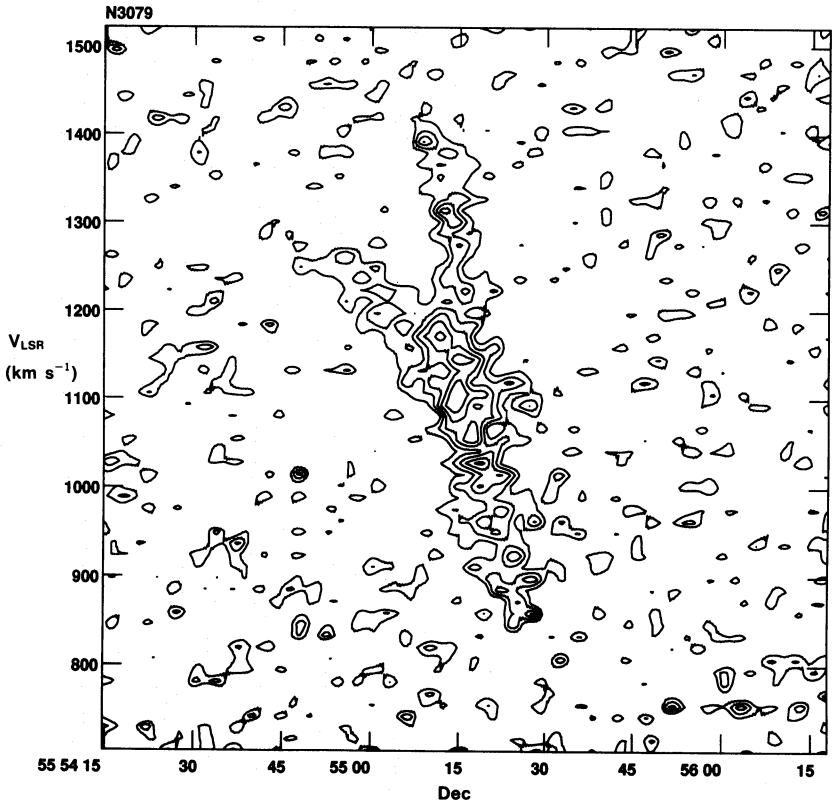

(d)

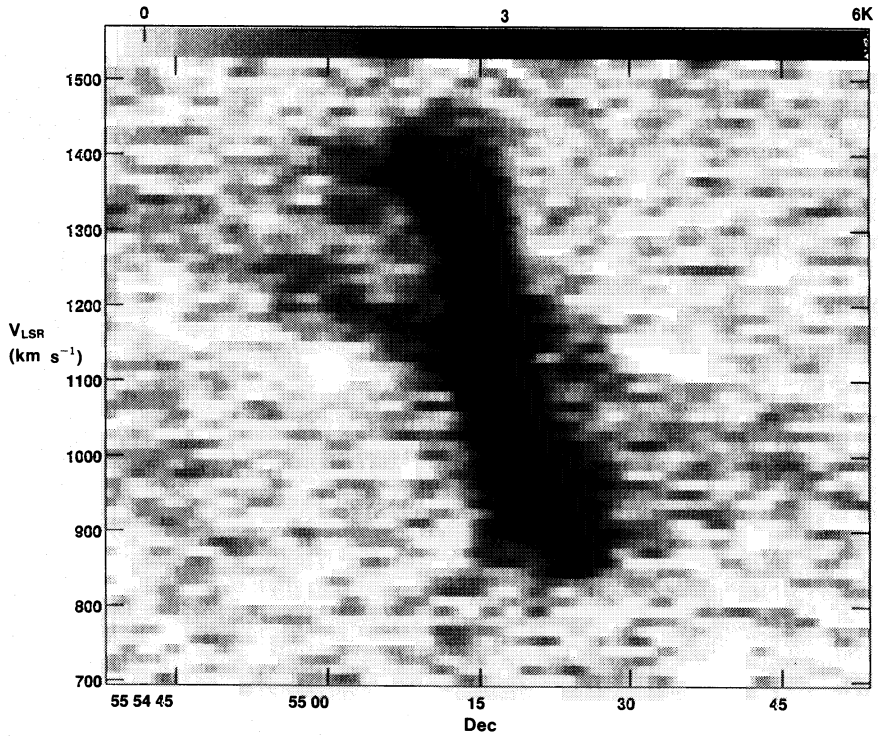

Fig. 5. (Continued)

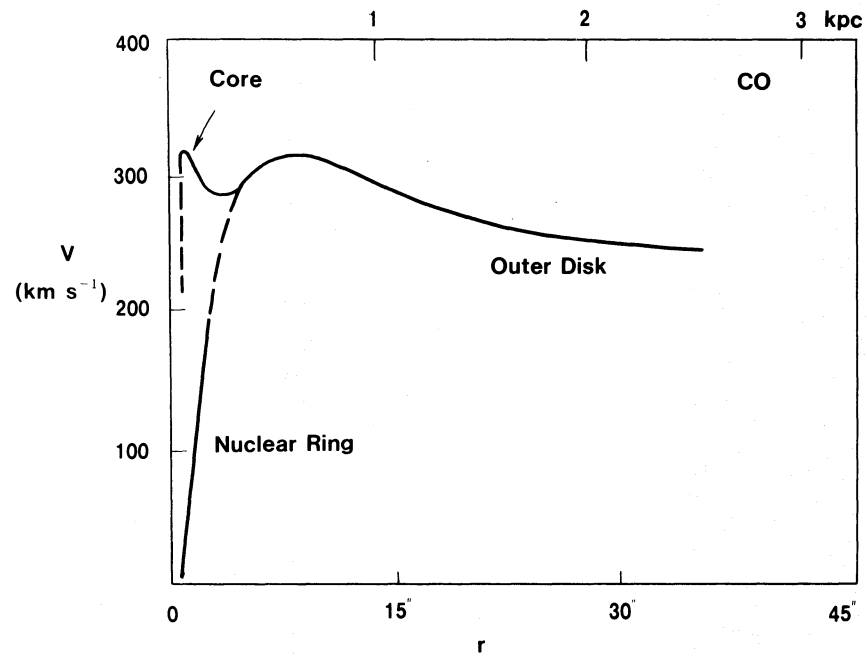

Fig. 6. Rotation curve of the inner region of NGC 3079 derived from the CO data.

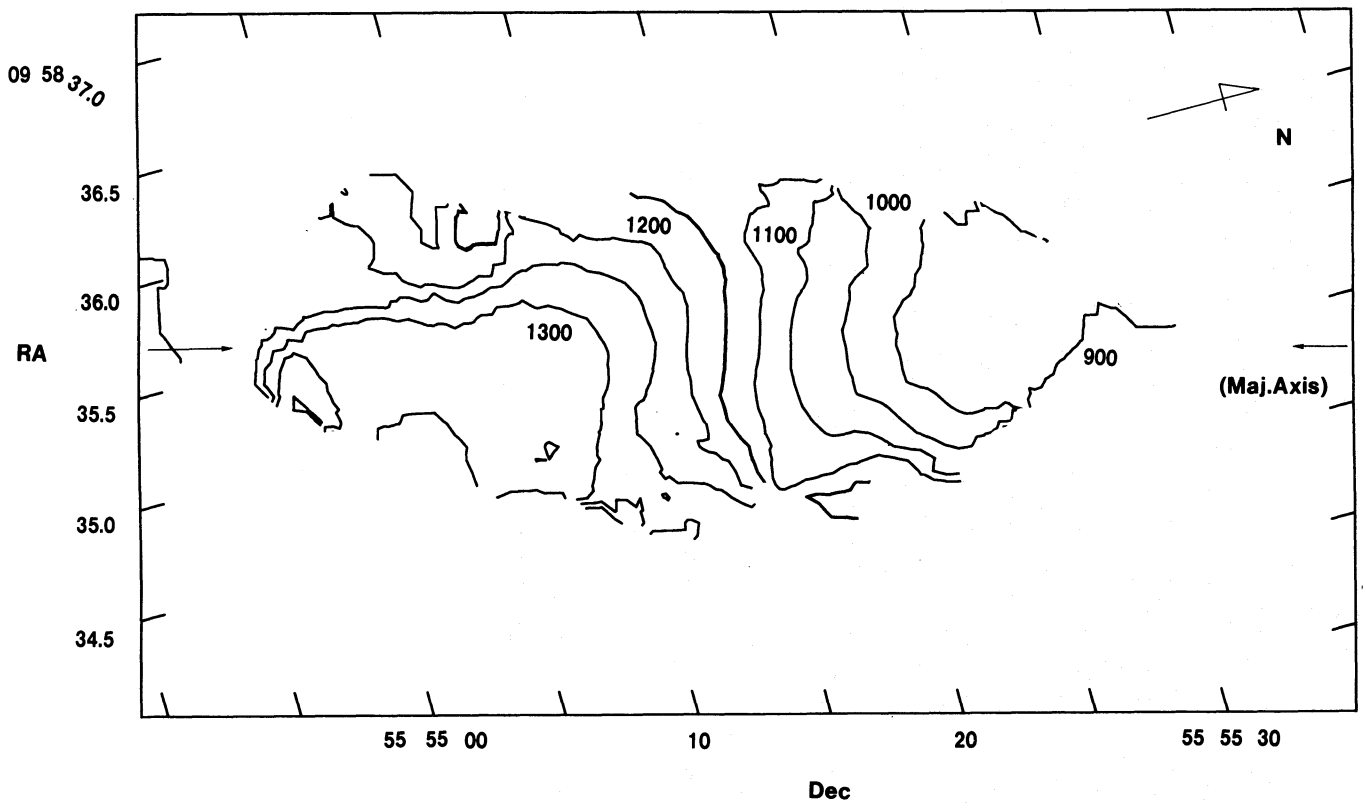

Fig. 7. Mean velocity field of NGC 3079. LSR velocities (km s^{-1}) are indicated on contours.

3.5. Velocity Field

Figure 7 shows the distribution of the mean velocities, as obtained from the 64-channel map cube, where the major axis is taken holizontal. The velocity field clearly indicates galactic rotation about the minor axis: rigid rotation of the nuclear disk region and a flatter rotation of the outer disk. Also remarkable in this figure is the asymmetry of the velocity distribution about the major axis in the outer disk. This is most clearly seen in the southern disk, where the velocity has a gradient of about 100 km s^{-1} (5″)$^{-1}$ perpendicular to the galactic plane. A similar asymmetry, but in an opposite sense, is recognized in the northern disk. We can also observe some kinks in velocity contours near the systemic velocity.

All of the features indicate that the galactic disk is siginificantly warped in the sense that the nodal line of the disk beyond radius 10″ (750 pc) is inclined by about +10° from the assumed major axis: namely, the outer disk has a nodal line at a position angle of −5°, approximately parallel to the north-south direction. It is peculiar that the inclination of the kinematical nodal line, as found here, is rather in the opposite direction from the inner warped nuclear disk, whose major axis is inclined by about −40° to the major axis: namely, the inner warped disk is inclined by about 50° from the outer disk, as determined from the kinematical nodal line. We could therefore even speculate that the inner warped disk is more likely to be out of the plane than the main disk.

Alternatively, the apparent asymmetry in the velocity field might be due to some noncircular motion of gas above the galactic plane, such as due to an ejection or contraction of gas perpendicular to the galactic disk. In this case, the disk plane would be inclined from the line of sight by some finite angular amount; the disk is not edge-on.

From the present data it is difficult to discriminate between the above two possibilities: in order to clarify the situation we need a more sensitive mapping of the outer disk.

3.6. Upper Limit to Continuum Flux of the Nucleus

Since our spectrometer covered a velocity range as wide as 835 km s^{-1}, we could determine the continuum level using emission outside the CO line profile. Using channel maps, an upper limit to the continuum peak flux density of 40 mJy beam^{-1} at 115 GHz has been obtained toward the nucleus at a resolution of 4″.07 × 3″.55. This can be compared with the continuum flux densities obtained from the VLA: 78 mJy beam^{-1} at 1.46 GHz at a 1″.4×1″.2 resolution (Duric and Seaquist 1988), 65 mJy beam^{-1} at 4.9 GHz at 1″.3 × 1″.1 resolution (Duric and Seaquist 1988), and 83 mJy beam^{-1} at 4.9 GHz at a 1″.3 × 1″.1 resolution (Duric et al. 1983). It may perhaps be better to compared it with the 1.4 GHz peak flux density of 138 mJy beam^{-1} at the about same resolution of 4″.3 × 3″.6 (Duric et al. 1983).

The spectral index toward the nucleus, as determined from 115 and 1.4 GHz observations with about identical beams (4.1–4″.3 × 3″.6) for the central compact core, is $\alpha < -0.28$ ($S_\nu \propto \nu^\alpha$). We may therefore conclude that the inverted spectral index ($\alpha = +0.15$) obtained between 1.4 and 4.9 GHz (Duric and Seaquist 1988) does not apply at our higher frequency: a cut off probably exists between 4.9 and 115 GHz; the data are, however, too crude to discuss details.

3.7. Molecular and Dynamical Masses

Our result is consistent with the previous ^{12}CO (1−0) observations from the Owens Valley mm-wave array at a 8″.3×6″.1 resolution, which already inferred the existence of a dense nuclear molecular disk within the central 14″ (Young et al. 1988). However, these latter data are incomplete, since the filter bank covered only 400 km s^{-1}, significantly less than the line width; a continuum level could thus not be established. The Owens Valley results revealed that a typical brightness temperature is ∼ 1 K. Our data have revealed a peak brightness temperature of about 0.17 Jy beam^{-1} = 5.1 K T_B on the integrated intensity map for the 700 km s^{-1}velocity range (figure 3). The highest peak brightness temperature has been observed at V_{LSR} = 1054 km s^{-1}, indicating as high as 1.43 Jy beam^{-1} = 9.3 K T_B .

With the usual (albeit uncertain) assumptions, the H_2 distribution and mass may be estimated, while adopting $N(H_2)/\int T_B dV = 4 \times 10^{20}$ cm^{-2} (K km s^{-1})$^{-1}$ (Young and Scoville 1982).

The velocity-integrated CO intensity at the nucleus is $I_{CO} = 3.5 \times 10^3$ K km s^{-1}. The CO column density toward the nucleus is therefore estimated to be about 1.4×10^{24} H_2 cm^{-2} = $2.2 \times 10^4 M_\odot$ pc^{-2}. Since the compact component is not resolved, the face-on column density would be of the same order as this. The mass of molecular gas within a spherical volume of diameter equal to the beam size (radius ∼ 150 pc for a 15.6 Mpc distance) is estimated to be as large as $\sim 1.4 \times 10^9 (D/15.6\ \mathrm{Mpc})^2 M_\odot$, and the mean molecular gas density is $\sim 3.4 \times 10^3 (D/15.6\ \mathrm{Mpc})^{-1}$ H cm^{-3}. An upperlimit to the dynamical mass for this component can be estimated to be $\sim 3 \times 10^9 M_\odot$ from the velocity dispersion, ∼ ±300 km s^{-1}, and the radius.

The H_2 mass involved within the rigidly rotating part of the nuclear disk at $r < 5''.4$ = 400 pc (where the averaged I_{co} is 2.1×10^3 K km s^{-1}) is estimated to be $\sim 5.4 \times 10^9 (D/15.6\ \mathrm{Mpc})^2 M_\odot$. The mean brightness temperature of the entire nuclear disk within a 30″ × 15″ area (within $r < 15'' = 1.1$ kpc) in figure 3 is estimated to be 8.4×10^2 K km s^{-1}. The mean column density for this area is therefore 3.4×10^{23} H_2 cm^{-2} = $5.7 \times 10^3 M_\odot$ pc^{-2}.

Hence, the total H_2 mass involved in this nuclear disk can be estimated to be $10.6 \times 10^9 (D/15.6\ \mathrm{Mpc})^2 M_\odot$. The H_2 mass is a factor of four greater than the previous value, $5.7 \times 10^9 (D/24\ \mathrm{Mpc})^2 M_\odot$, as obtained from the Owens Valley Array (Young et al. 1988).

The distribution of the total mass (dynamical mass) within the observed region can be obtained from the rotation characteristics of the CO gas. The nuclear disk between r =150 and 400 pc shows the rigid rotation, which is expressed as $V = 820(r\ \mathrm{kpc}^{-1})\ \mathrm{km\ s}^{-1}$. We therefore obtain the dynamical mass as $M \sim 1.9 \times 10^8 (r/100\ \mathrm{pc})^3 (D/15.6\ \mathrm{Mpc})^3 M_\odot$. The rotation velocity attains a maximum of $V \sim 330\ \mathrm{km\ s}^{-1}$ at $r = 400$ pc, and the mass involved within this radius is approximately $M_{\mathrm{dyn}} \sim 10.5 \times 10^9 (D/15.6\ \mathrm{Mpc})^2 M_\odot$. This is about twice the H_2 mass for the same region. The dynamical mass involved within the whole nuclear disk can be estimated from the rotation curve. The rotation velocity at the edge of the disk, $r = 15'' = 1.1$ kpc, is about 270 km s^{-1}. This leads to the dynamical mass of the nuclear disk as being $M \sim 1.8 \times 10^{10} (D/15.6\ \mathrm{Mpc})^2 M_\odot$, which is about 1.7-times the H_2 mass in the same area. It is thus shown that the molecular gas makes up 50 to 60% of the total (dynamical) mass of the nuclear disk; the same partially applies within the disk. This $M_{\mathrm{H_2}}/M_{\mathrm{dyn}}$ ratio is large compared to normal galactic disk, while also being rather typical for the central regions of CO and IR bright galaxies (e.g., Sofue 1988; Young and Scoville 1991).

3.8. Relationship with Radio Continuum Features

There should be some complex interplay between the ejection of the radio continuum lobes and jets from the nucleus (Duric et al. 1983; Duric and Seaquist 1988; Irwin and Seaquist 1988) and the dense nuclear gaseous disk and ring. Also, the morphology as well as kinematics of the gas disk should be affected by ejection. In order to investigate the relationship between the nuclear disk and the radio continuum features, we made overlays of the 6-cm continnum map from the VLA (Duric and Seaquist 1983) on our CO maps. Figure 8a is an overlay on the total intensity CO map; figure 8b is an overlay on the channel map at 1150 km s^{-1} (the CO systemic velocity) displaying the warped nuclear disk with the vertical spurs.

The central core and the nuclear disk in the total CO intensity map (figure 8a) shows excellent morphological agreement with those observed in the radio continuum. Moreover, there appears to be a positional coincidence between the directions of the radio lobes and the vertical spurs, which are also visible in this total CO intensity map. The vertical CO spurs are better "isolated" in the channel map (figure 8b), and the coincidence with the radio continuum lobe directions is more clearly seen in this figure. It is remarkable that the warped molecular disk, which is most likely the inner part of the rigidly rotating broad ring, lies almost perpendicular to the line connecting the north-eastern and south-western ridges of the radio continuum lobes. In fact, the brighter continuum ridges connecting the nucleus with the lobes are asymmetric with respect to the rotation axis of the galaxy. This lends support to the suggestion by Irwin and Seaquist (1988) that the nuclear jet is focussed in the perpendicular direction by the surrounding molecular gas.

4. Discussion

We have performed high-angular and velocity-resolution observations of the radio-lobe edge-on galaxy NGC 3079 in the ^{12}CO($J = 1-0$) line using the NMA. The molecular gas is distributed in a disk along the major axis, whose characteristics can be summarized as follows:

(i) An unresolved nuclear core of radius a few arc sec ($r < 200$ pc), which has a high velocity dispersion (~ 700 km s^{-1}). A sharp absorption feature due to a foreground molecular cloud in the outer disk or arm is superposed on the velocity profile.

(ii) A nuclear disk of radius ~ 750 pc, which shows depression in emission at the systemic velocity, indicating a broad ring structure of radius 190 pc. The major (inner) part of this nuclear ring is rotating rigidly with a maximum speed of 330 km s^{-1} at $r = 400$ pc.

(iii) The inner ($r < 400$ pc) part of the nuclear ring is significantly warped by about 40° from the major axis, approximately perpendicular to the main ridge connecting the radio continuum lobes and the nucleus.

(iv) The warped nuclear ring is associated with two vertical spurs extending in the direction of the radio lobes.

(v) The molecular mass of the nuclear disk makes up about 50–60% of the total (dynamical) mass.

(vi) The outer disk exhibits a feature in the position-velocity diagrams consistent with the exitence of spiral arms.

(vii) The mean velocity field shows a kinematical asymmetry about the major axis, which would suggest that the outer disk is warped in an opposite sense to the nuclear warped disk. Alternatively, it might be due to gas flows vertical to the galactic disk.

(viii) The molecular gas distribution shows good morphological agreement with the radio continuum morphology of the galactic disk.

(ix) The rotation curve as derived from terminal velocities on the (X, V) diagrams indicates a rigid rotation near the nuclear region and a flat galactic rotation at $V \sim 240$ km s^{-1} in the outer region.

The extent to which the nuclear gas participates undoubtedly plays a significant role in the origin and propagation of the radio lobes. Knowledge concerning the

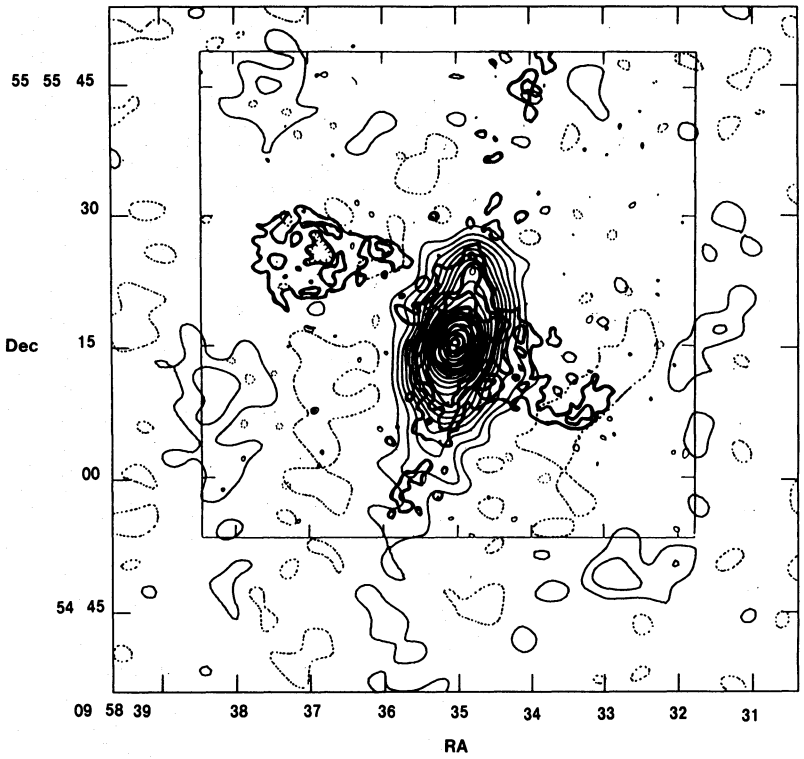

(a)

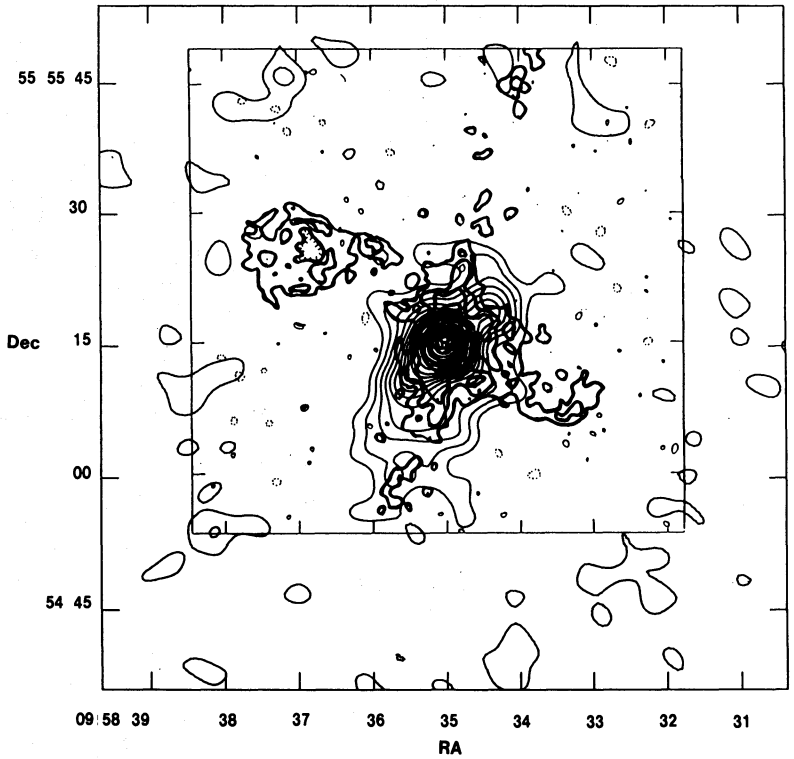

(b)

Fig. 8. Overlay of the 6-cm radio continuum map (Duric et al. 1983) on the CO intensity maps for (a) total intensity (figure 2), and (b) for the warped disk component from the channel map at $V_{\rm LSR}$ =1164 km s^{-1}(figure 3).

kinematics, morphology and density of the interstellar medium in the immediate nuclear vicinity is particularly important, since the ISM can fuel both the nucleus as well as focus, or confine, the outflow (Irwin and Seaquist 1988; Fabbiano et al. 1989). Indeed, the situation is not necessarily analogous to the more powerful radio galaxies, since the density and angular momentum of the gaseous component in spiral galaxies is considerably different from that in ellipticals. In order to investigate these relationships, it is important to observe each phase of the ISM with resolution which is high enough to "isolate" the affected gas. In this context we have isolated the H_2 gas distribution and its kinematics from the high-resolution CO observations. A detailed modeling of the results in relation to the ejection mechanism of the radio lobes is another topic of the project. For this purpose, however, we need some more data from other frequencies, which will be described in a separate paper.

In this respect we mention our comprehensive study of NGC 3079, which involves observations of CO in emission using the NRO interferometer, as well as H I and OH in absorption using the VLA in its highest resolution configuration. Lower resolution (C/D array) VLA observations of OH and H I have already been carried out (e.g., Irwin 1988), and matching resolution (A array) data have also been obtained (e.g., Irwin and Seaquist 1991). In addition, we will compare these results with Hα data which have already been obtained by other observers (e.g., Ford 1985). In each case, arcsecond resolution ($\sim$100 pc) is obtained and, with appropriate smoothing, both velocity and spatial resolutions can be matched, identically (with the possible exception of Hα in velocity). This permits a direct comparison of each (molecular, atomic, and ionized) gas phase of the ISM. Intercomparison of data from these observations, as well as a thourough discussion of the interrelationships between these components and the nuclear activity, will be given in a forthcoming paper. Obviously, another important aspect of the present project is the star-formation (or star burst) process in the nuclear region and its relation to the origin of the radio lobes. This topic will also be discussed in a separate paper.

This work was financially supported by the Ministry of Education, Science and Culture under Grant No. 01420001 and 01302009 (Y. Sofue) and the National Research Council Research Council of Canada (J. Irwin). Y. S. thanks E. Nishihara and Y. Murata for their technical assistance in data reduction.

References

Chikada, Y., Ishiguro, M., Hirabayashi, H., Morimoto, M., Morita, K.-I., Kanzawa, H., Iwashita, H., Nakazima, K., Ishikawa, S., Takahashi, T., Handa, K., Kasuga, T., Okumura, S., Miyazawa, T., Nakazuru, T., Miura, K., and Nagasawa, S. 1987, *Proc. IEEE*, **75**, 1203.

Duric, N., Seaquist, E. R., Crane, P. C., Bignell, R. C., and Davis, L. E. 1983, *Astrophys. J. Letters*, **273**, L11.

Duric, N., and Seaquist, E. R. 1988, *Astrophys. J.*, **326**, 574.

Eckart, A., Cameron, M., Rothermel, H., Wild, W., Zinnercker, H., Rydbeck, G., Olberg, M., and Wiklind, T. 1990, *Astrophys. J.*, **363**, 451.

Fabbiano, G., Gioia, I. M., and Trinchieri, G. 1989, *Astrophys. J.*, **347**, 127.

Ford, H. C., Crane, P. C., Jacoby, G. H., Lawrie, D. G., and van der Hulst, J. M. 1985, *Astrophys. J.*, **293**, 132.

Haschick, A. D., and Baan, W. A. 1985, *Nature*, **314**, 144.

Hummel, E., van Gorkom, J. H., and Kotanyi, C. G. 1983, *Astrophys. J. Letters*, **267**, L5.

Irwin, J. A. 1988, Ph. D. Thesis, University of Toronto.

Irwin, J. A., and Seaquist, E. R. 1988, *Astrophys. J.*, **335**, 658.

Irwin, J. A., and Seaquist, E. R. 1991, *Astrophys. J.*, **371**, 111.

Irwin, J. A., Seaquist, E. R., Taylor, A. R., and Duric, N. 1987, *Astrophys. J. Letters*, **313**, L91.

Irwin, J. A., and Sofue, Y. 1992, *Astrophys. J. Letters*, in press.

Israel, F. P., van Dischoeck, E. F., Baas, F., Koornneef, J., Black, J. H., and de Graauw, T. 1990, *Astron. Astrophys.*, **227**, 342.

Nakai, N., Hayashi, M., Handa, T., Sofue, Y., Hasegawa, T., and Sasaki, M. 1986, *Publ. Astron. Soc. Japan*, **38**, 603.

Nakai, N., Hayashi, M., Handa, T., Sofue, Y., Hasegawa, T., and Sasaki, M. 1987, *Publ. Astron. Soc. Japan*, **39**, 685.

Sofue, Y. 1988, in *Molecular Clouds in the Milky Way and External Galaxies*, ed. R. L. Dickman, R. L. Snell, and J. S. Young (Spirnger-Verlag, Berlin), p. 375.

Young, J. S., Claussen, M. J., and Scoville, N. Z. 1988, *Astrophys. J.*, **324**, 115.

Young J. S., and Scoville, N. Z. 1982, *Astrophys. J.*, **258**, 467.

Young J. S., and Scoville, N. Z. 1991, *Ann. Rev. Astron. Astrophys.*, in press.

Véron-Cetty, M.-P., and Véron, P. 1985, *Astron. Astrophys.*, **145**, 425.